ELSEVIER

Journal of Fluids and Structures 22 (2006) 979–988

JOURNAL OF FLUIDS AND STRUCTURES

www.elsevier.com/locate/jfs

Numerical investigation of the flow around two circular cylinders in tandem

B.S. Carmo, J.R. Meneghini*

NDF, "Escola Politécnica", Department of Mechanical Engineering, University of São Paulo, CEP 05508-900 São Paulo, SP, Brazil

Received 22 September 2005; accepted 7 April 2006
Available online 24 July 2006

Abstract

The incompressible flow around pairs of circular cylinders in tandem arrangements is investigated in this paper. The spectral element method is employed to carry out two- and three-dimensional simulations of the flow. The centre-to-centre distance (l_{cc}) of the investigated configurations varies from 1.5 to 8 diameters (D), and results thus obtained are compared to the isolated cylinder case. The simulations are in the Reynolds number (Re) range from 160 to 320, covering the transition in the wake. Our analysis focuses on the small-scale instabilities of vortex shedding, which occurs in the Re range investigated. With the aid of Strouhal data and vorticity contours, we propose mechanisms to explain the interference phenomenon and its interaction with the three-dimensional vortical structures present in the flow field. It is found that, for $\mathrm{Re} > 190$, when three-dimensional structures are present in the flow field, two-dimensional simulations are not sufficient to predict the (Re, l_{cc}) pair of drag inversion.

Keywords: Interference; Transition; Bluff body; Vortex shedding

1. Introduction

The flow around pairs of circular cylinders has been the subject of many investigations. The flow interference that occurs in such configurations is responsible for changes in the fluid loads and in important features of the flow field. In addition, investigations of the flow around pairs of cylinders can provide a better understanding of the vortex dynamics, pressure distribution and fluid forces in cases involving more complex arrangements.

Among the many possible arrangements in which two circular cylinders can be positioned relatively to a cross-flow, one that has been extensively studied is the tandem arrangement, as sketched in Fig. 1. In this configuration, the type of interference present is *wake interference*, where the wake of the upstream cylinder touches the downstream one (Zdravkovich, 1987). The effect of this interference is seen, for example, in the variation of the Strouhal number (St) and force coefficients with the Reynolds number (Re) and with the centre-to-centre distance (l_{cc}). The Strouhal number is the nondimensional frequency of vortex shedding and is defined as follows: $\mathrm{St} \equiv fD/U_\infty$, where f is the dimensional frequency in Hz.

Many of the previous works regarding the flow around two circular cylinders identified diverse *interference regimes* and were based primarily on flow visualization in experiments. Investigations such Igarashi (1981), Zdravkovich (1987)

*Corresponding author. Tel.: +55 11 3091 5641; fax: 55 11 3091 5642.
E-mail address: julio.meneghini@poli.usp.br (J.R. Meneghini).

0889-9746/$ - see front matter © 2006 Elsevier Ltd. All rights reserved.
doi:10.1016/j.jfluidstructs.2006.04.016

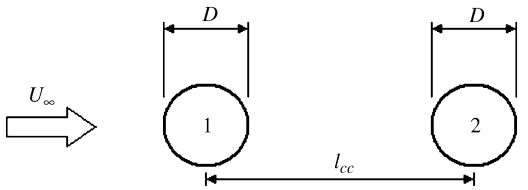

Fig. 1. Schematic drawing of the flow around two cylinders in a tandem arrangement.

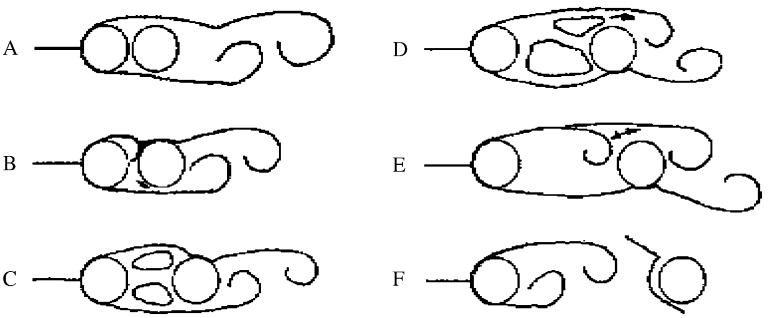

Fig. 2. Interference regimes in the flow around pairs of circular cylinders in tandem arrangements. Extracted and adapted from Igarashi (1981).

and Sumner et al. (2000) proposed classifications of these regimes. The classification of Igarashi (1981) deals essentially with tandem arrangements, and therefore is the one we adopt here. According to this classification, six different interference regimes can be identified (Fig. 2): (A) the free shear layers that originate from the separation on the surface of the upstream cylinder do not re-attach to the surface of the downstream cylinder; (B) the shear layers that come from the upstream cylinder are captured by the downstream one, but there is no vortex formation in the gap between the bodies; (C) symmetric vortices are formed between the cylinders; (D) the symmetric vortices become unstable and start to grow in proximity to the downstream cylinder; (E) the shear layers originating from the upstream cylinder roll up very near the downstream cylinder; and (F) the near wake region (formation region) ends before the downstream body and vortices are shed in the gap region in a regular way.

From regime A to regime D, the drag coefficient in the downstream cylinder is considerably lower than in the upstream cylinder. This can be understood when we note that, from A to D, the downstream cylinder is inside the near wake behind the upstream cylinder and therefore is in a low pressure region. In these cases, the drag in the second cylinder is usually negative. When the flow is in regime F, the drag in the downstream cylinder is positive. The spacing at which the downstream cylinder drag changes sign is called *drag inversion spacing* or *critical spacing*, and it depends on the Re.

These experimental results motivated a number of computational studies with the purpose of reproducing the interference regimes and achieving a better understanding of flow interference. For example, Slaouti and Stansby (1992) utilized a discrete vortex method to carry out two-dimensional simulations, while Meneghini et al. (2001) employed a two-dimensional finite element formulation. Both studies show good qualitative agreement with experimental data, in the sense that the interference regimes are identified. Additionally, they present some important insights with respect to the physical mechanisms of the wake interference. However, the quantitative results presented differ from experimental data for $\mathrm{Re} \geqslant 200$. We believe this to be due to the existence of three-dimensional structures in the flows at such Re, as discussed below.

To the best of our knowledge, the only published work that deals with three-dimensional features in the flow around circular cylinders in tandem is the investigation by Wu et al. (1994). In this study, experiments were carried out in which flow visualization and hot wire anemometry were employed to measure the spanwise coherence at certain points in the wake. The results show that the flow is clearly three-dimensional for all l_{cc} investigated and also that the coherence values differ from those found in the flow around a single cylinder. It is clear, therefore, that three-dimensional structures play a crucial role in the flow interference.

Our study focuses on the three-dimensional wake transition in flows around two circular cylinders in tandem arrangements. We are concerned with the two small-scale instabilities, referred to as mode A and B. According to

Williamson (1996), who investigated such instabilities for an isolated circular cylinder case, mode A is a three-dimensional instability with a spanwise wavelength of around 3–4 diameters, and mode B has a smaller wavelength of about 1 diameter.

In the present investigation two- and three-dimensional numerical simulations of the flow around a pair of cylinders and around a single cylinder for $160 \leqslant \mathrm{Re} \leqslant 320$ are carried out, using an extremely accurate and high-order finite element method. Comparing graphs of St as a function of Re and l_{cc} and with the aid of field contour plots, we discuss the role of the three-dimensional structures in the flows with wake interference and the differences with reference to the single cylinder case. Also, we present in detail some of the two-dimensional mechanisms involved in the flow interference.

This paper is organized as follows: a brief description of the numerical method used in the simulations is given in Section 2. In Section 3, results concerning convergence tests and validation of the methodology are presented. In Section 4, we report the results of the simulations and investigate their possible implications. In Section 5, conclusions are drawn regarding the interaction between the flow interference and the three-dimensional vortical structures that arise in the wake transition.

Additional results obtained concerning force and correlation coefficients will be reported in forthcoming papers.

2. Methodology

We consider the motion of a viscous fluid past infinitely long circular cylinders placed perpendicular to a uniform free stream. The fluid is assumed to have constant density ρ and constant dynamic viscosity μ. The idealized incompressible flow depends on the following parameters: the cylinder diameter D, the free-stream speed U_∞, and the kinematic viscosity of the fluid $\nu \equiv \mu/\rho$. The only nondimensional combination of these parameters is the Reynolds number, defined in this paper as $\mathrm{Re} \equiv U_\infty D/\nu$, where U_∞ is the free-stream velocity, D is the cylinder diameter, and ν is the kinematic viscosity. Re serves as the control parameter for the system. The problem may be described in dimensionless variables, with U_∞ and D serving as the reference scales for velocity and distance. The state of the fluid at any time t as it moves past the cylinder is determined by the velocity field $\mathbf{u}(x, y, z, t)$ and the pressure field $p(x, y, z, t)$. These fields are described in a coordinate system where x is aligned with the free stream direction, y is normal to the free stream, and z is along the span of the cylinder. The evolution of the flow is described by the incompressible Navier–Stokes equations.

The computational domain Ω represents a region of three-dimensional space surrounding the cylinder that contains the 'important' part of the flow, as determined by convergence tests. The equations were discretized in space by means of a high-order spectral element method described in Karniadakis and Sherwin (1999). In the flow around infinitely long cylinders is a situation where there is a direction which does not have a characteristic length. Our approach was to use an *hp* discretization in the plane perpendicular to the cylinder utilizing Jacobi polynomials as basis functions, and a pure *p* expansion in the spanwise direction utilizing Fourier series. This approach has some advantages in terms of computational efficiency, for example the ease of implementing the code for parallel processors. The algorithms implemented are described in detail in Karniadakis and Sherwin (1999) and the discretization in time followed the scheme presented by Karniadakis et al. (1991).

3. Convergence tests and validation

A first set of convergence tests were carried out in order to achieve a proper computational domain for the cross-sectional plane (plane xy). We chose the flow around a sole cylinder as the test case. We employed a procedure similar to that presented by Barkley and Henderson (1996) to attain an adequate domain for two-dimensional simulations in terms of extension and discretization. The parameters tested were the degree of the basis function and the lengths of the inflow, outflow and side regions. The final meshes used an eighth order Jacobi polynomial as basis function and had between 336 and 468 elements, depending on the configuration. The fluid domains extended $36D$ upstream from the upstream cylinder, $45D$ downstream from the downstream cylinder and $50D$ sidewise from the central line that links the cylinder centres. Fig. 3 shows a comparison between the results obtained with the final mesh and experimental data provided by Williamson (1989). It can be seen that our results agree very well with this experimental data; the error is lower than 1%.

Subsequently, convergence tests for the parameters related exclusively to three-dimensional simulations were carried out. These parameters were the number of modes in the Fourier expansion employed in the spanwise direction and the periodic length of the cylinder. The first parameter is directly related to the small-scales representation. After many

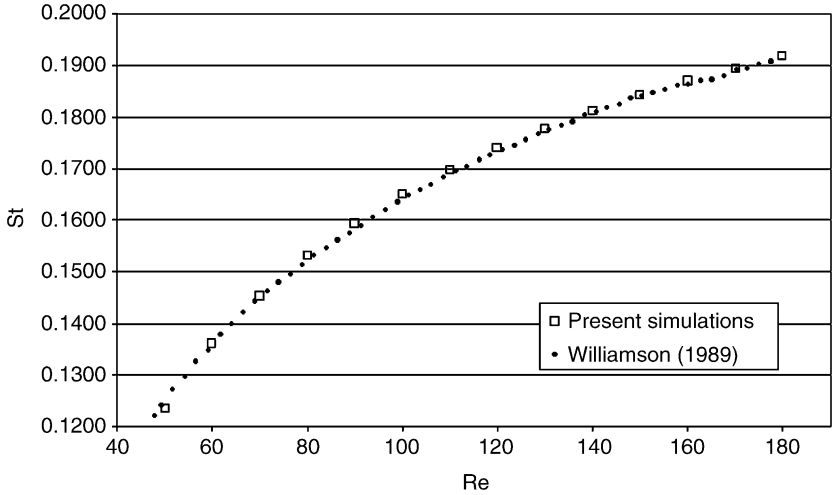

Fig. 3. Comparison of Strouhal number from two-dimensional calculations and measured by Williamson (1989).

Table 1
Periodic length convergence tests, Re = 200

Periodic length	St	$\bar{C_D}$
3*D*	0.196	1.33
5*D*	0.196	1.31
8*D*	0.195	1.29
12*D*	0.184	1.28
18*D*	0.185	1.27
Experimental results		
Williamson (1996)	0.183	
Fey et al. (1998)	0.183	
Wieselsberger (1922)		1.27–1.30

simulations at the highest Re investigated (320), we concluded that a discretization of approximately 6.4 modes per diameter length in the spanwise direction was sufficient to achieve an adequate representation of the flow. The value of the second parameter, the periodic length, is linked to the maximum wavelength that can be reproduced in the spanwise direction. A periodic boundary condition was employed at the ends of the cylinders, such that the maximum wavelength of an instability that could be represented would be the chosen periodic length. The results for these cases are shown in Table 1, in which a sudden drop in the Strouhal number can be seen when the periodic length changes from 8*D* to 12*D*. This drop is related to the representation of large-scale vortex dislocations [see Williamson (1992)]. As explained before, in the present work we are concerned with the small-scale instabilities, mode A and mode B. Therefore, we chose a periodic length of 5 diameters for the simulations, and 64 modes for the discretization of the equations in this direction. Further work addressing the issue of large-scale instabilities is in progress.

4. Results and discussion

Flows around a single cylinder and around two cylinders in tandem with a centre-to-centre distance l_{cc} of 1.5*D*, 3*D*, 3.5*D*, 5*D* and 8*D* were simulated. These configurations are denoted, respectively, as *1cyl*, *t1.5d*, *t3d*, *t3.5d*, *t5d* and *t8d*. The Reynolds numbers tested were 160, 195, 200, 240, 270, 300 and 320, hence covering the Re range of the transition in the wake. In this work, we present the results of the Strouhal number for these simulations. We calculate St from the

peak of the spectrum of the lift coefficient. In all cases the St obtained for the upstream and downstream cylinder were the same. Relying on field contours, time histories and spectra of physical quantities, we suggest some hypotheses to explain the variation of St with Re and l_{cc}, in a phenomenological fashion. Some observations concerning the changes in the wake transition with the configuration are also made.

4.1. Two-dimensional results

The two-dimensional simulation results are shown in Fig. 4, in which it can be seen that all configurations show a similar behaviour in respect to the variations of Re, the exceptions being the spacing of $3D$ and $3.5D$. While the curves of all the other configurations always present a positive slope, the *t3d* case shows a decrease between Re = 240 and 270, followed by a jump to a much higher value of St at the next point, Re = 300; and the *t3.5d* case shows a jump between Re = 200 and 240. This behaviour is caused by the *drag inversion* that occurs for these configurations, evidenced by the vorticity contours in Fig. 5, where one can clearly observe how the near wake of the first cylinder is influenced by the presence of the second one. For Re = 270, where a bistable regime takes place, it is interesting to note that there is a higher number of near peaks in the lift coefficient spectrum when compared with the results for Re = 240 and 300.

Another aspect that deserves attention in Fig. 4 is the difference between the slope of the curves in cases where $l_{cc} < l_{cc}^{C}$. For *t1.5d* the slope of the graph is higher than for *t3d* and *t3.5d*, the last two being almost parallel. This occurred because we were dealing with two different regimes, as one can observe in Fig. 6. The simulations with $l_{cc} = 1.5D$ resulted in the regime C, where symmetric vortices appeared in the region between the cylinders, while in the simulations with configurations *t3d* and *t3.5d*, when $l_{cc} < l_{cc}^{C}$ the regime that was observed was regime D. In these last two cases, for a given Re, the St of the configuration *t3.5d* was lower than the St of *t3d* because vortices were shed as only one formation region existed. In addition, we believe that, since for $l_{cc} = 3.5D$ the downstream cylinder is positioned in a way that more circulation remains retained between the bodies, the shear layer that is originated in the second cylinder has less circulation and therefore this flow has a lower St.

Another point worthwhile noting is that the graphs relative to the configurations *1cyl*, *t5d* and *t8d*, presented in Fig. 4 show the same behaviour, but a systematic difference in the values is observed along the entire Re range investigated. This occurred because there is of proximity interference from the downstream cylinder on the upstream one; in other words, even after the drag inversion, the downstream body continued to influence the resulting forces in the upstream cylinder. Fig. 7 shows the velocity and pressure values along the central line ($y = 0$) of the mean fields of simulations with Re = 300 and it can be seen that the pressure field in the near wake of the upstream cylinder is modified by the presence of the second body; moreover, the nearer the cylinders, the higher the pressure in the near wake. These results suggest that a high pressure in the near wake makes the vortex shedding from the upstream cylinder more difficult, and this diminishes St. That is why in Fig. 4 we see that, for a given Re, for example 300, and analyzing the cases with regime F, the Strouhal number decreases with the diminution of l_{cc}.

A final point concerning the two-dimensional simulations is the synchronization of St that occurred in flows in regime F. In this regime, there was no true formation region behind the downstream cylinder, and vortices were shed directly from its surface. It appears, therefore, that it is not the dynamics in the near wake that determines the shedding

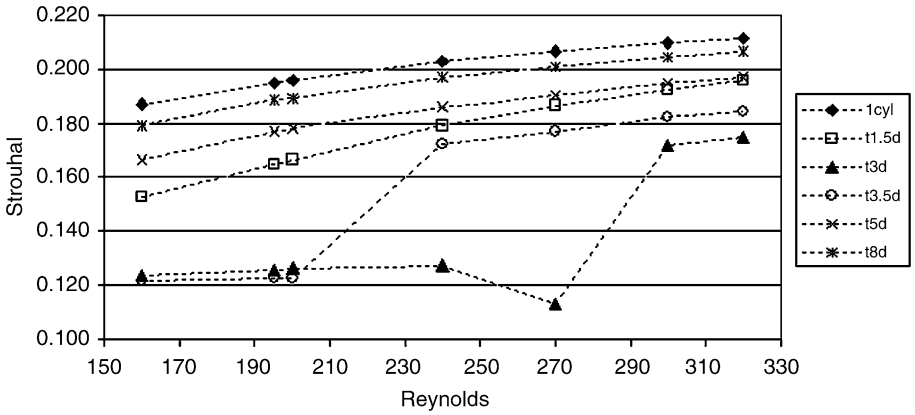

Fig. 4. Strouhal number as a function of the Reynolds number: two-dimensional simulations.

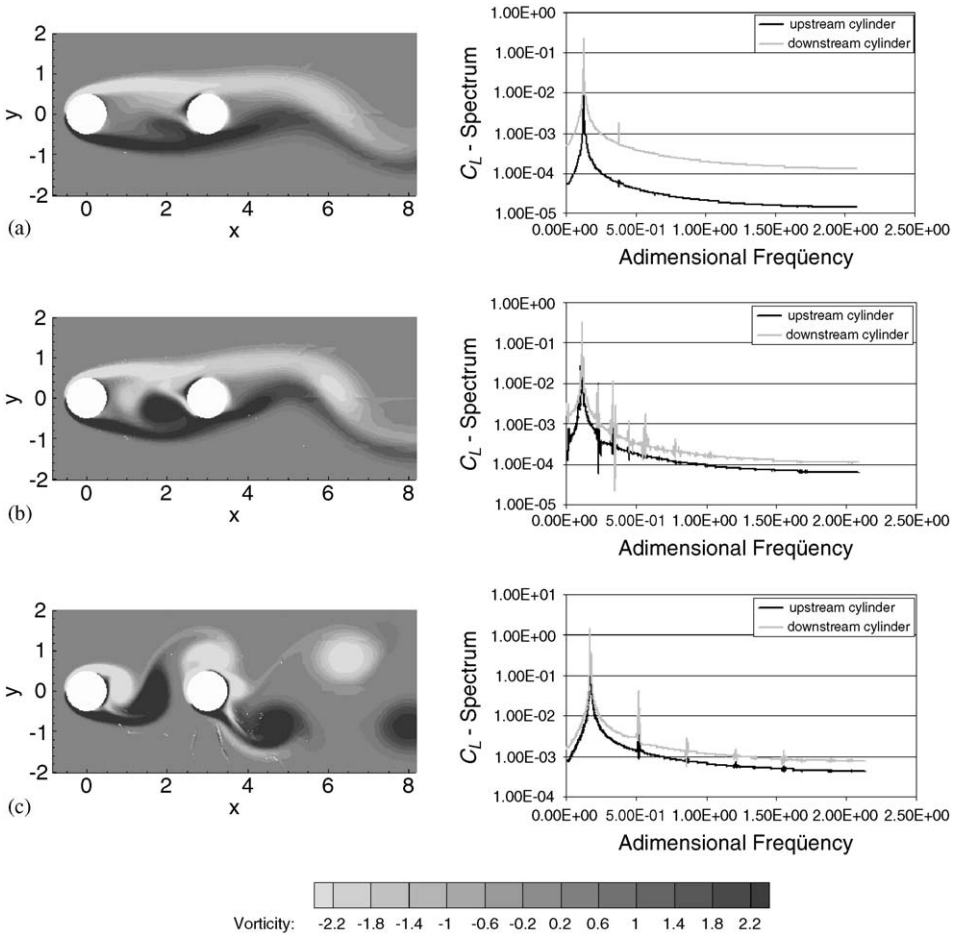

Fig. 5. Vorticity contours and C_L spectra, centre-to-centre distance $3D$ (*t3d* case), two-dimensional simulations: (a) Re = 240; (b) Re = 270; and (c) Re = 300. Vorticity has been nondimensionalized by the cylinder radius.

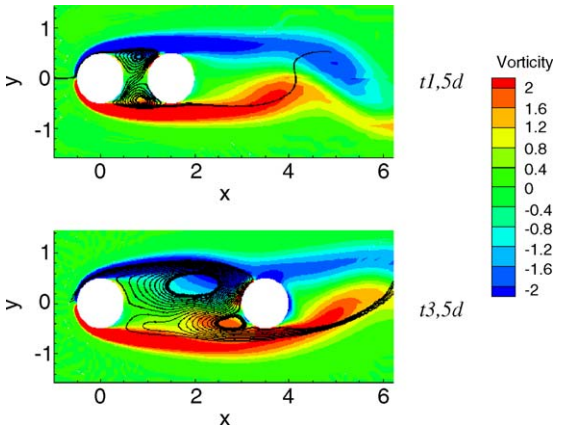

Fig. 6. Vorticity contours and instantaneous emission lines, Re = 200, two-dimensional simulations.

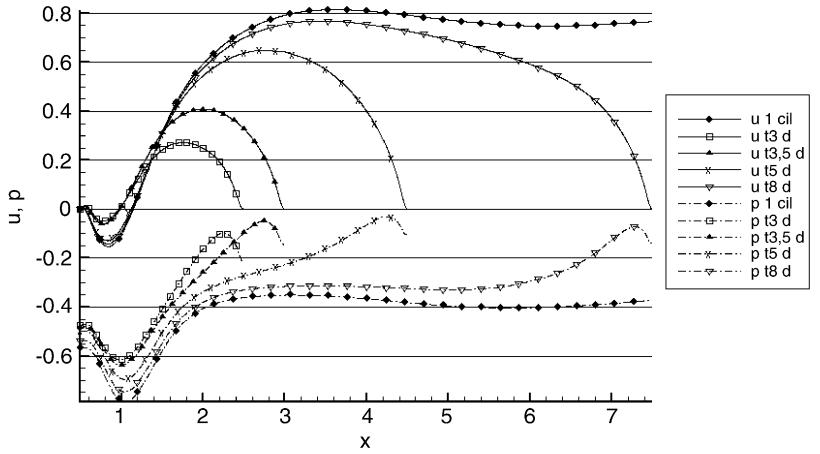

Fig. 7. Velocity and pressure along the $y = 0$ line of mean fields. Two-dimensional simulations, Re = 300.

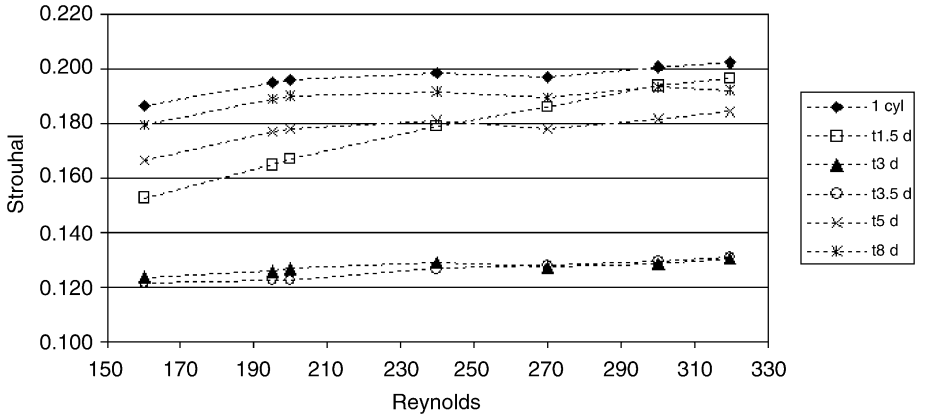

Fig. 8. Strouhal number as a function of the Reynolds number, three-dimensional simulations.

frequency of the downstream body, but rather the incident oscillatory flow; the alternate vortices that hit the body force the shedding in the downstream cylinder to occur at the same frequency.

4.2. Three-dimensional results

Three distinct behaviours can be observed in Fig. 8. The first is represented by the configurations *1cyl*, *t5d*, and *t8d*, the second by *t1.5d*, and the third by *t3d*, and *t3.5d*. Each of these behaviours will be analyzed below.

The graphs of the two-dimensional simulations relative to the cases that show the first kind of behaviour (*1cyl*, *t5d* and *t8d*) present a positive slope along the entire Re range (see Fig. 4), while the three-dimensional results seen in Fig. 8 exhibit lower St for $\mathrm{Re} > 200$. This phenomenon is also verified in experiments with an isolated cylinder and can be explained by the triggering of mode A (Williamson, 1996). As can be observed in Fig. 9, the appearance of three-dimensional structures leads to an increase in the formation length, and the St decreases. An important conclusion that can be drawn from the similarities of the behaviours of *1cyl*, *t5d* and *t8d* is that a spacing of $5D$ is large enough for the transition in the wake to occur in a analogous way to that observed in the flow around an isolated cylinder.

In the second kind of behaviour, observed for the case *t1.5d*, the plotting of the three-dimensional results produces a graph with positive slope for the entire Re range. Moreover, the graphs of two- and three-dimensional simulations are almost coincident. With the aim of verifying the existence of three-dimensional flow, we traced time histories of the velocity vector component in the z direction, referred to as w, at certain points in the wake region. One example can be

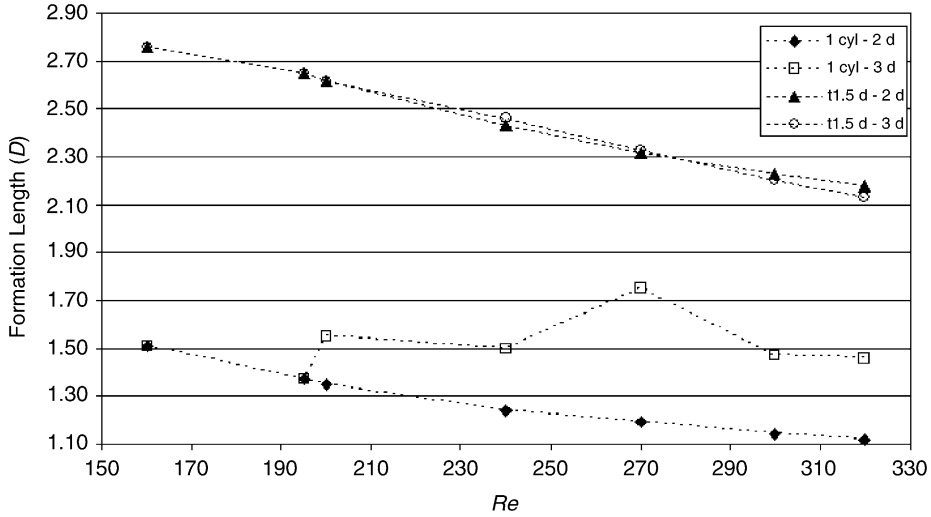

Fig. 9. Formation length for the cases *1cyl* and *t1.5d*, two- and three-dimensional simulations. This length is measured from the centre of the downstream cylinder.

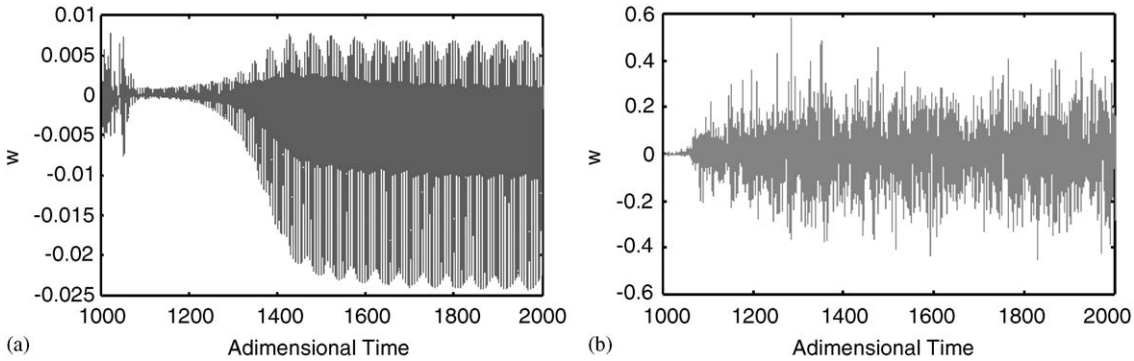

Fig. 10. Time histories of the w component of the velocity for Re = 300: (a) case *t1.5d* at point (12.92, −0.63, 2.42) and (b) case *t5d* at point (16.42, −0.63, 2.42), three-dimensional simulations.

seen in Fig. 10, where configurations *t1.5d* and *t5d* are compared, in flows with Re = 300. The x distance between the probes and the downstream cylinder was the same for both configurations and in both cases the flow is truly three-dimensional. However, the w amplitudes that are observed in the time history for *t1.5d* are considerably lower than those for *t5d*.

Fig. 11 shows instantaneous vorticity iso-surfaces for configurations *t1.5d*, *t3d* and *t5d*, Re = 270. Observing this figure, one can note that in *t1.5d* the three-dimensional structures, which in this figure are represented by the x-vorticity, are formed in a region relatively far from the second body, and there is no three-dimensional flow in the gap between the cylinders. In the other two cases, there are three-dimensional structures between the bodies, and they hit the second cylinder. It is known that the first three-dimensional instability, mode A, originates in the cores of the primary vortices (Williamson, 1996). In Fig. 9, we see that the formation length for *t1.5d* is considerably longer than that for *1cyl*. Therefore, for *t1.5d*, when the primary vortices are formed and the three-dimensional structures begin to appear, the shear layers are more diffused. this being the case, the structures that emerge will have lower intensity and less influence on the two-dimensional characteristics of the flow.

The graphs relative to *t3d* and *t3.5d* are examples of the third kind of behaviour. In these cases, in the two-dimensional simulations, a discontinuity was observed, caused by the drag inversion. However, this discontinuity was not observed in the curves generated by the three-dimensional results in the Re range investigated. In Fig. 11, we see that for the case *t3d* there is three-dimensional flow in the gap between the bodies and, although the vortices are not

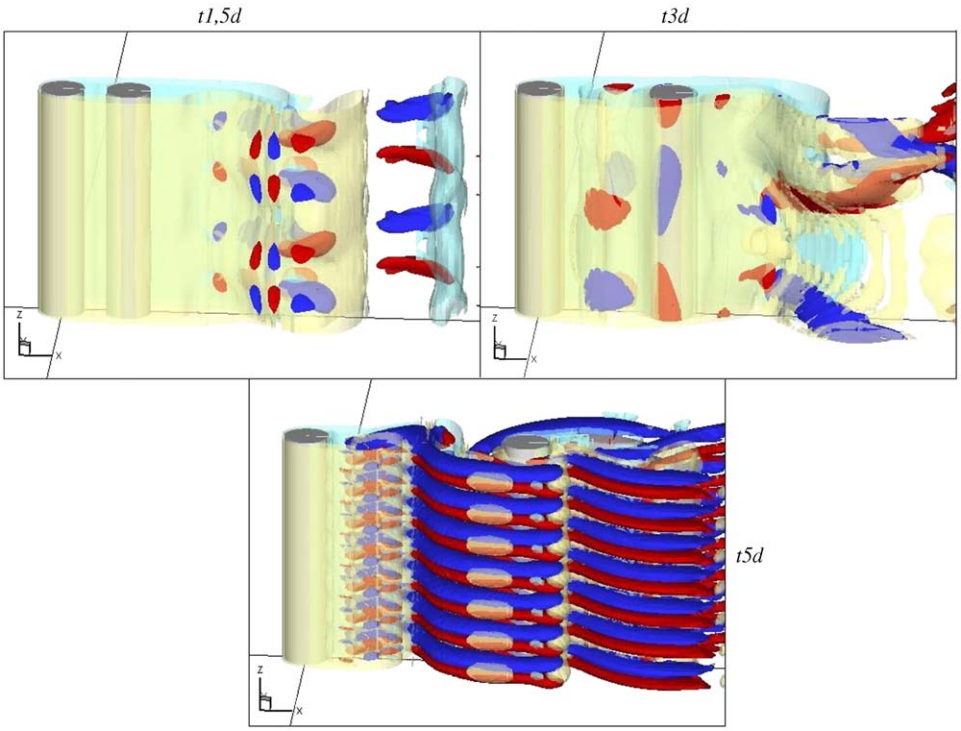

Fig. 11. x-vorticity (ω_x) and z-vorticity (ω_z) iso-surfaces, three-dimensional simulations, Re = 270. Dark blue surfaces correspond to $\omega_x = -1.0$, the red ones to $\omega_x = 1.0$, the transparent yellow ones to $\omega_z = 1.0$ and the transparent light blue ones to $\omega_z = -1.0$.

completely shed in this region, they begin to form there and, consequently, so do the three-dimensional structures. The formation length increases due the presence of such structures, and as a result, the drag inversion does not occur for this spacing. Bearing this in mind, we draw the conclusion that two-dimensional simulations are not sufficient to predict the (Re, l_{cc}) pair of the drag inversion.

5. Conclusions

A central goal of this work was to achieve a deeper understanding of the physical mechanisms that are involved in the interference phenomenon, especially those related to the presence of three-dimensionalities in the wake. With the aid of St data and vorticity contours, we propose mechanisms to explain the interference phenomenon and its interaction with the three-dimensional vortical structures present in the flow field and our conclusions are below.

The consequences of the presence of three-dimensional structures in the flow vary according to the interference regime. For a configuration in regime C, we verified that the St data obtained by means of two- and three-dimensional simulations are almost identical throughout the entire Re range investigated. Although the three-dimensional structures were present, they were very weak and were formed in a region far from the cylinders; consequently, they had very little influence on the forces that act on the bodies. In the cases of regime D, the three-dimensional simulations showed that there were three-dimensional structures in the region between the bodies. Comparing the two- and three-dimensional graphs that refer to *t3d* and *t3.5d*, we observed drag inversion in the Re range investigated for the two-dimensional simulations, but not for the three-dimensional ones. Finally, in regime F, which was observed for $l_{cc} \geqslant 5D$, the three-dimensional structures altered the forces on the cylinders in a similar way to that observed in the single cylinder case, as evidenced by the similar shapes of the curves relative to *1cyl*, *t5d* and *t8d* in Fig. 8.

We conclude that, for $\mathrm{Re} > 190$, two-dimensional simulations are not sufficient to predict the (Re, l_{cc}) pair of drag inversion, and thus they are not able to determine the interference regime for a given configuration in the vicinity of the critical spacing. Furthermore, depending on the interference regime, the existence of three-dimensional vortical

structures may significantly alter the fluid loads on the cylinders and, therefore, it is necessary to perform three-dimensional simulations to calculate the forces correctly.

Acknowledgements

The authors would like to acknowledge the financial support of Fapesp, FINEP and CNPq, and to Dr Spencer Sherwin, for providing the Nektar code at an early stage of this research project.

References

Barkley, D., Henderson, R.D., 1996. Three-dimensional Floquet stability analysis of the wake of a circular cylinder. Journal of Fluid Mechanics 322, 215–241.

Fey, U., König, M., Eckelmann, H., 1998. A new Strouhal–Reynolds number relationship for the circular cylinder in the range $47 < \mathrm{Re} < 2 \times 10^5$. Physics of Fluids 10 (7), 1547–1549.

Igarashi, T., 1981. Characteristics of the flow around two circular cylinders arranged in tandem. Bulletin of JSME 24 (188), 323–331.

Karniadakis, G.E., Sherwin, S.J., 1999. Spectral/hp Element Methods for CFD. Oxford University Press, New York.

Karniadakis, G.E., Israeli, M., Orzag, S.A., 1991. High-order splitting methods for the incompressible Navier–Stokes equations. Journal of Computational Physics 97, 414–443.

Meneghini, J.R., Saltara, F., Siqueira, C.L.R., Ferrari Jr., J.A., 2001. Numerical simulation of flow interference between two circular cylinders in tandem and side-by-side arrangements. Journal of Fluids and Structures 15, 327–350.

Slaouti, A., Stansby, P.K., 1992. Flow around two circular cylinders by the random-vortex method. Journal of Fluids and Structures 6, 641–670.

Sumner, D., Price, S.J., Païdoussis, M.P., 2000. Flow-pattern identification for two staggered circular cylinders in cross-flow. Journal of Fluid Mechanics 411, 263–303.

Wieselsberger, C., 1922. Numerical experiments in homogeneous turbulence. NACA Technical Note 84.

Williamson, C.H.K., 1989. Oblique and parallel modes of vortex shedding in the wake of a circular cylinder at low Reynolds numbers. Journal of Fluid Mechanics 206, 579–627.

Williamson, C.H.K., 1992. The natural and forced formation of spot-like 'vortex dislocations' in the transition of a wake. Journal of Fluid Mechanics 243, 393–441.

Williamson, C.H.K., 1996. Three-dimensional wake transition. Journal of Fluid Mechanics 328, 345–407.

Wu, J., Welch, L.W., Welsh, M.C., Sheridan, J., Walker, G.J., 1994. Spanwise wake structures of a circular-cylinder and 2 circular-cylinders in tandem. Experimental Thermal and Fluid Science 9 (3), 299–308.

Zdravkovich, M.M., 1987. The effects of interference between circular cylinders in cross flow. Journal of Fluids and Structures 1, 239–261.